HER2-targeting two-dimensional black phosphorus as a nanoplatform for chemo-photothermal therapy in breast cancer

Yuanke Liang [a,1], Jinxing Liu [b,1], Cong Zhao [b], Hexing Sun [a], Kaiyuan Huang [a], Qin Xie [c], De Zeng [c], Haoyu Lin [a,**], Benqing Zhou [b,*]

[a] Department of Thyroid and Breast Surgery, Clinical Research Center, The First Affiliated Hospital of Shantou University Medical College, Shantou, 515000, China
[b] Department of Biomedical Engineering, College of Engineering, Shantou University, Shantou, 515063, China
[c] Cancer Hospital of Shantou University Medical College, Shantou, 515031, China

ARTICLE INFO

ABSTRACT

Trastuzumab (Tmab) targeted therapy or its combination with chemotherapy is normally insufficient to elicit a comprehensive therapeutic response owing to the inherent or acquired drug resistance and systemic toxicity observed in highly invasive HER2-positive breast cancer. In this study, we propose a novel approach that integrates photothermal therapy (PTT) with targeted therapy and chemotherapy, thereby achieving additive or synergistic therapeutic outcomes. We utilize PEGylated two-dimensional black phosphorus (2D BP) as a nanoplatform and photothermal agent to load chemotherapeutic drug mitoxantrone (MTO) and conjugate with Tmab (BP-PEG-MTO-Tmab). The *in vitro* and *in vivo* experiments demonstrated that the HER2-targeting BP-PEG-MTO-Tmab complexes exhibited desirable biocompatibility, safety and enhanced cancer cell uptake efficiency, resulting in increased accumulation and prolonged retention of BP and MTO within tumors. Consequently, the complex improved photothermal and chemotherapy treatment efficacy in HER2-positive cells *in vitro* and a subcutaneous tumor model *in vivo*, while minimized harm to normal cells and showed desirable organ compatibility. Collectively, our study provides compelling evidence for the remarkable efficacy of targeted and synergistic chemo-photothermal therapy utilizing all-in-one nanoparticles as a delivery system for BP and chemotherapeutic drug in HER2-positive breast cancer.

1. Introduction

Breast cancer is the most common malignancy type in the world and the leading cause of cancer death among women [1]. However, due to the high heterogeneity of breast cancer, the treatment strategies and prognosis of breast cancer in different molecular subtypes are different [2]. The molecular subtype of HER2 (human epithermal growth factor receptor 2) overexpression occurs in about 20–40% of breast cancer [3, 4]. Although it is highly aggressive and metastatic, molecular targeted therapy with humanized monoclonal antibody trastuzumab (Tmab) in combination with chemotherapy significantly improves prognosis, reducing the risk of recurrence by 46% and mortality by 33% in patients with early HER2-positive breast cancer [5]. However, the development of resistance reduces the therapeutic index of Tmab. In the process of Tmab treatment, about 70% of breast cancer patients have primary or

secondary drug resistance, especially a considerable part of them will develop brain metastases, which is a difficult problem in clinical treatment [6]. Despite Tmab treatment showing drug resistance or low HER2 expression, recent clinical research findings have demonstrated that novel antibody-drug conjugate (ADC) drugs such as Tmab-deruxtecan (DS-8201a) display a significant therapeutic efficacy [7,8]. These results underscore the continued significance of combining novel chemotherapeutic drug strategies with Tmab for further management of Tmab-resistant HER2-positive breast cancer [9,10].

Though Tmab-deruxtecan exhibited 79.7% overall response and showed a relatively considerable reduction in tumor burden, about 20% of patients have no benefit from treatment [11]. This suggested that achieving complete eradication of breast cancer solely through chemotherapy and/or targeted therapy could be challenging due to the inherent limitations associated with these therapeutic approaches.

---

* Corresponding author.
** Corresponding author.
   E-mail addresses: rainlhy@stu.edu.cn (H. Lin), bqzhou@stu.edu.cn (B. Zhou).
[1] Authors contributed equally to this work.

Recently, photothermal therapy (PTT) has emerged as an innovative cancer treatment approach, utilizing the thermal energy generated from the absorption of optical energy by light-absorbing agents localized in the tumor, thereby facilitating tumor ablation [12,13]. Therefore, combination PTT with targeted therapy or chemotherapy presents potential avenues for leveraging the benefits and mitigating the drawbacks of each therapeutic modality, thereby enhancing antitumor therapeutic effect [14].

Nanotechnology has great potential in the field of combination therapy, as nanoplatforms can serve as multiple carriers to integrate various drugs for various therapeutic modalities [15–23]. As a new single element material, two-dimensional black phosphorus (2D BP) has high mobility, anisotropy and adjustable band gap properties, and has been widely used in catalytic energy, photoelectric devices and biomedical materials [24–30]. 2D BP as a good photothermal reagent has excellent photothermal conversion efficiency of 28.4–38.8% in near infrared region, and is widely used for cancer PTT or PTT-based combination therapy [31–41]. Compared with other 2D nanomaterials (such as graphene and MoS_2, etc.), 2D BP has a higher specific surface area and unique multi-fold structure, which can effectively support proteins, liposomes, drug molecules and nanoparticles [42–44]. In addition, 2D BP can be formed into different sizes by mechanical stripping, liquid stripping and pulsed laser deposition, which can be completely metabolized into non-toxic phosphates and phosphonates *in vivo*, showing desirable biocompatibility [45–47]. However, naked BP is easily degraded by light, oxygen, and water, which will significantly affect the photothermal property of BP [15]. Therefore, naked BP should be modified to increase its stability before biomedical applications, such as polyethylene glycol (PEG) [34], polydopamine [48], poly-lactic-*co*-glycolic acid (PLGA) [49], titanium sulfonate ligand [50], and hydrogel [41] modifications. It was found that 2D BP quantum dots (BPQDs) encapsulated by polylactic-*co*-glycolic acid (PLGA) microspheres for PTT of tumors by emulsifying solvent volatilization [49]. The polymer shell formed by PLGA can isolate BPQDs from the physiological environment, ensuring the stable performance of BPQDs in the treatment process. After treatment, BPQDs will be slowly released and degraded along with the gradual degradation of PLGA shell, and then safely metabolized out of the body, showing excellent biodegradability and compatibility. In addition, 2D BP with multi-fold structure can effectively load chemotherapeutic drugs, such as doxorubicin (DOX), and the DOX loading content was as high as 950% (weight ratio of drug to carrier) [51], which was much higher than most other drug carriers [52].

In this study, we used PEGylated 2D BP (BP-PEG) as a photothermal agent and nanocarrier to load chemotherapeutic drug mitoxantrone (MTO) and modify Tmab for combined molecular targeted therapy with chemo-photothermal therapy of HER2-positive breast cancer. Herein, PEG modification can enhance the stability and biocompatibility of 2D BP [34]. Besides, since naked BP is easily degraded in aqueous solution, the colloidal and photothermal stability of BP can be significantly improved through Tmab modification [53]. UV–vis absorption spectroscopy and zeta potential data showed that 2D BP effectively loaded with MTO and successfully modified by Tmab. The formed BP-PEG-MTO-Tmab complexes significantly targeted HER2-positive cancer cells *in vitro* and *in vivo*. Under NIR laser irradiation, the complexes can effectively destroy HER2-positive cancer cells *in vitro* and *in vivo*, thereby effectively inhibiting tumor growth. This study provides a new idea for the precise combination therapy of breast cancer, especially HER2-positive breast cancer.

2. Materials and methods

2.1. Materials

BP crystalline powder was purchased from XFNANO Technology Co. Ltd. (Nanjing, China). 1-Methyl-2-pyrrolidinone (NMP) and MTO were

obtained from Sigma-Aldrich, Inc. (St. Louis, MO). Methoxy polyethylene glycol amine (mPEG-NH_2, molecular weight = 2000) was acquired from Ponsure Biological (Wuhu, China). Tmab was purchased from Genentech Inc. (South San Francisco, CA). RPMI-1640 medium, Dulbecco's Modified Eagle Medium (DMEM), fetal bovine serum, 0.25% trypsin-EDTA, and penicillin/streptomycin were obtained from Gibco (Grand Island, NY). Calcein-AM/PI double stain kit and cell counting kit-8 (CCK-8) were purchased from Dojindo Laboratories (Kumamoto, Japan). SK-BR-3 cells were purchased from the American Type Culture Collection (ATCC), and 4T1 cells were obtained from Procell Life Science &Technology Co., Ltd. (Wuhan, China). All cell lines were mycoplasma-free and were authenticated using short tandem repeat (STR) profiling.

2.2. Synthesis of BP-PEG-MTO-Tmab

BPQDs were prepared using the method of liquid phase exfoliation [5,32]. Then, the BPQDs (1 mg/mL, 1 mL) were mixed with mPEG-NH_2 (1 mg/mL, 5 mL) and placed in ultrasonic cleaning instrument for 30 min, and stirred strongly for 4 h in dark conditions [34]. MTO (1 mg/mL, 0.2 mL) was then added to the above solution and stirred over night to form BP-PEG-MTO using the unique fold structure of BPQDs. Lastly, Tmab (3 mg/mL, 1 mL) was added to BP-PEG-MTO solution and stirred for another 12 h to form BP-PEG-MTO-Tmab through electrostatic interaction.

2.3. In vitro MTO release

The release kinetics of MTO was determined by measuring MTO absorbance at 609 nm using a UV–vis spectrophotometer (UV-1780, Shimadzu, Japan). BP-PEG-MTO-Tmab (0.8 mL) at the MTO concentration of 0.5 mg/mL was put into the dialysis bag with an interception molecular weight of 8000–14000. The dialysis bag was then immersed in 7.2 mL of PBS (pH 7.4) or acetic acid buffer (pH 5.5) and placed in a constant temperature shaker with a vibration speed of 100 rpm at 37 °C. At each predetermined time point, 0.5 mL of outerphase solution was removed from each vial for quantitative analysis using UV–vis spectroscopy. An equal volume of fresh corresponding buffer solution was replenished to the vial to keep the outer phase volume constant.

2.4. In vitro cytotoxicity assay

SK-BR-3 and 4T1 cells (5000 cells per well) were seeded into a 96-well plate. After overnight incubation, the cells were cocultured with BP-PEG-Tmab, BP-PEG-MTO-Tmab, and free MTO at different concentrations for 24 h. Then, a standard CCK-8 assay was performed to obtain relative cell viability according to the manufacturer's instructions.

2.5. In vitro PTT

SK-BR-3 and 4T1 cells were seeded into a 6-well plate at a density of 5×10^5 cells/well and cultured overnight. Then the cells were cocultured with BP-PEG-MTO-Tmab at different concentrations for 6 h, and the cells were collected in 1.5 mL-tubes without medium *via* digestion and centrifugation. Then the cells were cultured for another 2 h and stained with trypan blue (Hyclone; Logan, UT), followed by a TC20TM Automated Cell Counter (Bio-Rad, Hercules, CA) for cell counting. Similarly, the treated cells were stained by calcein-AM/PI double staining kit according to the manufacturer's instructions, and observed by an inverted fluorescence microscope (Leica, Wetzlar, Germany) to further evaluate *in vitro* PTT efficacy of BP-PEG-MTO-Tmab.

2.6. In vitro targeting assay

To evaluate *in vitro* specific targeting of BP-PEG-MTO-Tmab complexes using confocal laser scanning microscopy (CLSM), we first
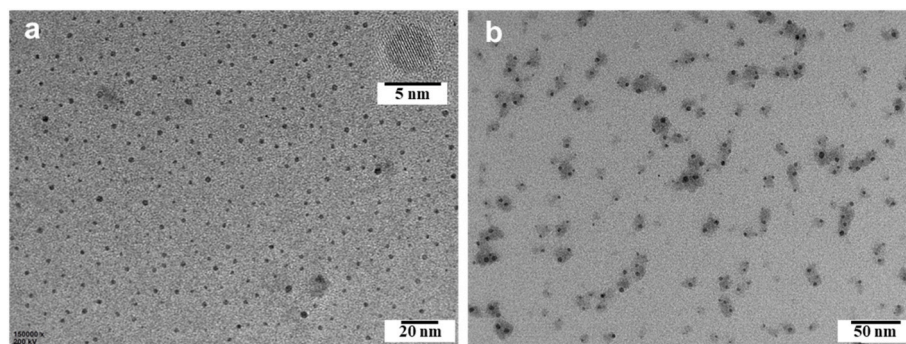
Fig. 1. (a, b) TEM images of 2D BP (a) and BP-PEG-MTO-Tmab complexes. Inset in the panel (a) show the high-resolution TEM image of 2D BP.

synthesized FITC fluorescence labeled BP-PEG-MTO-Tmab. The synthetic method of BP-PEG-FITC-MTO-Tmab is the same as that of BP-PEG-MTO-Tmab, only replacing mPEG-NH$_2$ with FITC-PEG-NH$_2$. SK-BR-3 cells (2×10^5 cells/well) as one type of HER2-positive cells were seeded into a 12-well plate and cultured overnight. Then the cells were cocultured with BP-PEG-FITC-MTO and BP-PEG-FITC-MTO-Tmab for 1 h. The cells were washed by PBS twice and fixed by paraformaldehyde, and the nucleus and cytoskeleton were respectively stained by DAPI and phalloidin before CLSM imaging.

Likewise, 4T1 (HER2-negative cells) and SK-BR-3 cells respectively treated with BP-PEG-MTO-Tmab complexes for 6 h, and directly observed under an inverted microscope to further investigate the specific phagocytic effect of cells on the complexes.

2.7. Plasmid and lentivirus infection

The pLV-Her2 lentiviral plasmid was purchased from Sino Biological Inc. (Beijing, China). pLV-Her2 lentiviral vector together with pVSV-G and pHR package vectors were transfected in to HEK293T cells by

using Lipofectamine 3000 (Thermo Fisher Scientific, MA) and cultured for 48 h. The supernatants of cell medium containing virus were collected and infected 4T1 cells with polybrene and selected in medium containing 1 μg/mL puromycin for HER2 stable expressing cell model (4T1-Her2 cells).

2.8. Immunofluorescence assay

4T1 and 4T1-Her2 cells were washed three times with PBS and fixed in 4% paraformaldehyde for 15 min and permeabilized with 0.5% Triton X-100 in PBS followed by blocking with 5% BSA in PBS for 60 min at room temperature. Subsequently, cells were incubated with HER2 primary antibody (#2165, Cell Signaling Technology, MA) follow by Alexa Fluor-conjugated secondary antibodies (Thermo Fisher Scientific, MA). Finally, cells were stained with DAPI (Thermo Fisher Scientific, MA) and mounted with ProLong Gold and Diamond Antifade Mountant. Images were captured with an immunofluorescence microscope (Carl Zeiss, Germany).
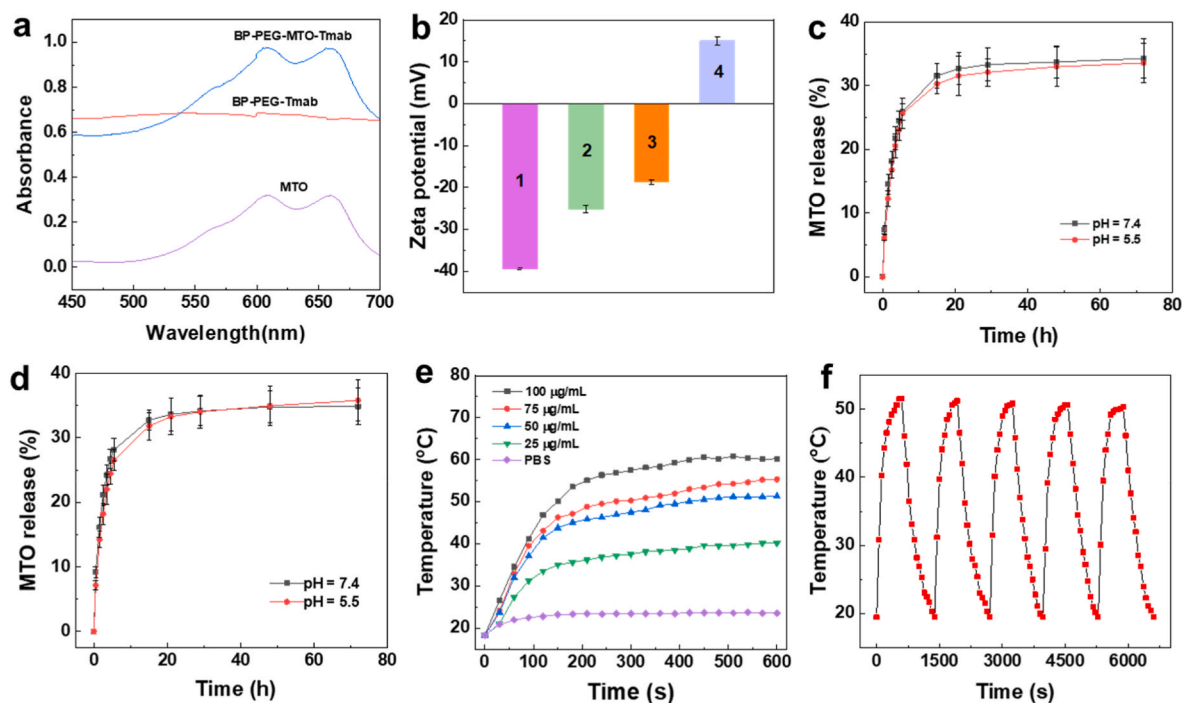

Fig. 2. (a) UV–vis spectra of MTO, BP-PEG-Tmab, and BP-PEG-MTO-Tmab, respectively. (b) Zeta potentials of naked BP (1), BP-PEG (2), BP-PEG-MTO (3), and BP-PEG-MTO-Tmab (4). (c, d) Cumulative MTO release curve of BP-PEG-MTO (c) and BP-PEG-MTO-Tmab (d) in different pHs at 37 °C. (e) Temperature rise curve of BP-PEG-MTO-Tmab with different BP concentrations irradiated by an 808 nm laser (1.0 W/cm^2) for 10 min. (f) Heating of BP-PEG-MTO-Tmab with a BP concentration of 50 μg/mL under an 808 nm laser irradiation at 1.0 W/cm^2 for five laser on/off cycles.
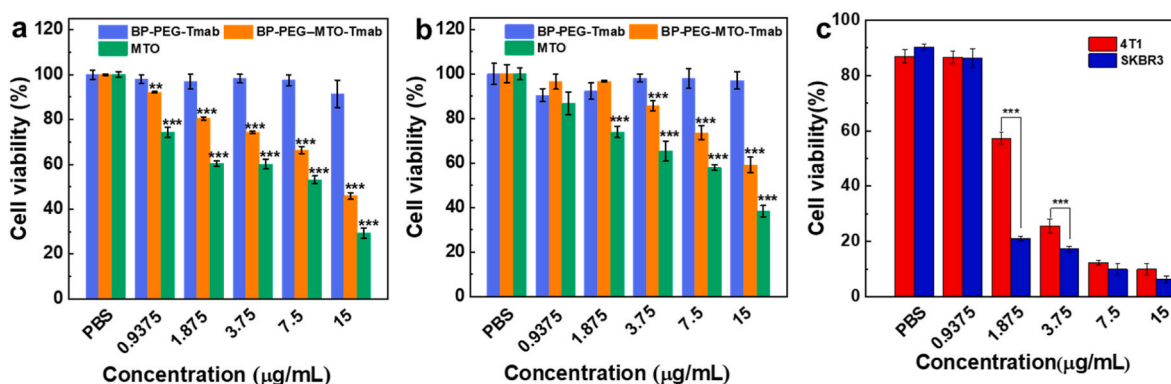
Fig. 3. (a, b) CCK-8 method was used to analyze the cell viability of SK-BR-3 (a) and 4T1 (b) treated with BP-PEG-Tmab, BP-PEG-MTO-Tmab, and free MTO at different concentrations (**p < 0.01, ***p < 0.001, vs. BP-PEG-Tmab group). (c) The cytotoxicity of SK-BR-3 and 4T1 cells were cocultured with BP-PEG-MTO-Tmab at different concentrations for 6 h and irradiated with an 808 nm laser (1.0 W/cm^2) for 10 min before measurement by a cell counter.

2.9. Immunoblot analysis

Immunoblotting was performed as previous study [54]. Briefly, proteins were extracted using RIPA buffer and quantified with a Bio-Rad BCA kit. Cell lysate was separated with SDS-PAGE gel and electro-transferred to PVDF membrane. Membranes were washed and incubated with primary antibodies and HRP-conjugated secondary antibody (Cell Signaling Technology, MA). The protein chemiluminescent signals were visualized using a ECL Western blotting substrate (Thermo Fisher Scientific, MA).

2.10. Animal models

The protocols and procedures for mice experiments were approved by the Animal Care and Use Committee of Shantou University Medical College (SUMC2021-226). Six-week-old Balb/C female mice (Charles River Laboratories, Beijing, China) were implanted with 2×10^5 4T1-Her2 cells. When tumor volume (width^2 × length/2) reached 100 mm^3, mice were randomly divided into groups as indicated and intravenously injected with BP hybrid nanodrugs. After that, mice were anesthetized and visualized with IVIS Kinetic In Vivo Image System (PerkinElmer, MA) or irradiated with an 808 nm laser. Tumor volume was measured every 2 days and mice were euthanized when tumor size met the institutional euthanasia criteria.

2.11. Immunohistochemical staining

Paraffin-embedded tumor samples were sectioned and baked at 60 °C for 2 h. After deparaffinization, hydration, antigen retrieval, and blocking of endogenous peroxidase, slides were incubated with Ki67 antibody (#9449, Cell Signaling Technology, MA) at 4 °C overnight, and HRP-conjugated secondary antibody (Maxim, Fujian, China) were used for incubation for 1 h at room temperature, followed by staining with DAB and counterstained with hematoxylin according to manufacturer's protocol. For hematoxylin and eosin (H&E) staining, sections were deparaffinized and hydrated. Finally, slides were stained with hematoxylin and eosin, respectively.

2.12. Statistical analysis

The statistical significance of all the data was performed by the one-way ANOVA. A P value of <0.05 was considered statistically significant, and *p < 0.05, **p < 0.01, ***P < 0.001.

3. Results and discussion

3.1. Synthesis and characterization of BP-PEG-MTO-Tmab

We used liquid phase exfoliation technique to prepare 2D BP. Transmission electron microscope (TEM) images showed that the formed 2D BP displayed good dispersion and had a diameter of 2.25 ± 0.56 nm (Fig. 1a and Fig. S2a). It was further confirmed by atomic force microscope (AFM) image (Fig. S1). High resolution TEM indicated that the 2D BP displayed distinct crystal structure (inset in Fig. 1a). TEM images of BP-PEG-MTO-Tmab complexes showed that the complexes had a diameter of 3.30 ± 0.86 nm (Fig. S2b), and 2D BP was effectively coated by Tmab protein (Fig. 1b), which significantly protected BP from water and air degradation [53]. As shown in Fig. 2a, the BP-PEG-MTO-Tmab displayed two peaks at 600–700 nm, which were the characteristic absorption peaks of MTO. It indicated that MTO was successfully loaded onto the surface of BP. Based on the standard calibration curve of MTO solution, the MTO loading efficiency (weight of MTO in the BP-PEG-MTO-Tmab/theoretical amount of MTO) was 63.4% (Fig. S3). This result was further confirmed by zeta potential analysis. As shown in Fig. 2b, the zeta potential of naked BP was −39.4 mV, which gradually increased after PEG modification (BP-PEG, −25.2 mV) and MTO loading (BP-PEG-MTO, −18.7 mV). Due to the positive charge of Tmab, the zeta potential of BP-PEG-MTO-Tmab was reversed to 15 mV after Tmab modification (Fig. 2b). These results indicated that 2D BP was successfully modified with PEG and Tmab, and effectively loaded with chemotherapeutic drug MTO. By Pierce™ bicinchoninic acid (BCA) protein assay, the load efficiency of Tmab protein was measured to be 19.7%, and the mass ratio of Tmab to BP was 0.59:1 according to the standard curve for BSA protein in the BCA protein assay [53]. For *in vitro* MTO release, as shown in Fig. 2c, under both PBS and acidic pH conditions, the cumulative release rate of MTO at 72 h was about 34%. After Tmab modification, the cumulative release rate of MTO under different pH conditions was also about 34% (Fig. 2d), indicating that the release of MTO in BP-PEG-MTO-Tmab was not affected by Tmab modification. It should be noted that with the passage of time, the MTO drug release slowed down, and the cumulative drug release will continue to increase, in agreement with the literature [18,34,51].

To verify the photothermal efficacy of BP-PEG-MTO-Tmab complexes, the complexes at BP different concentrations were lasered by an 808 nm NIR irradiation (LR-MFJ-808, Changchun laser technology Co., LTD., Changchun, China). As shown in Fig. 2e, the temperature of the complexes with a concentration of 50 μg/mL rose above 50 °C under an 808 nm laser irradiation (1.0 W/cm^2) for 10 min, while the temperature of PBS was 25 °C under the same conditions. Furthermore, the heating effect was better with the increase of the concentrations of complexes. Additionally, thanks to the modification of Tmab, the complexes
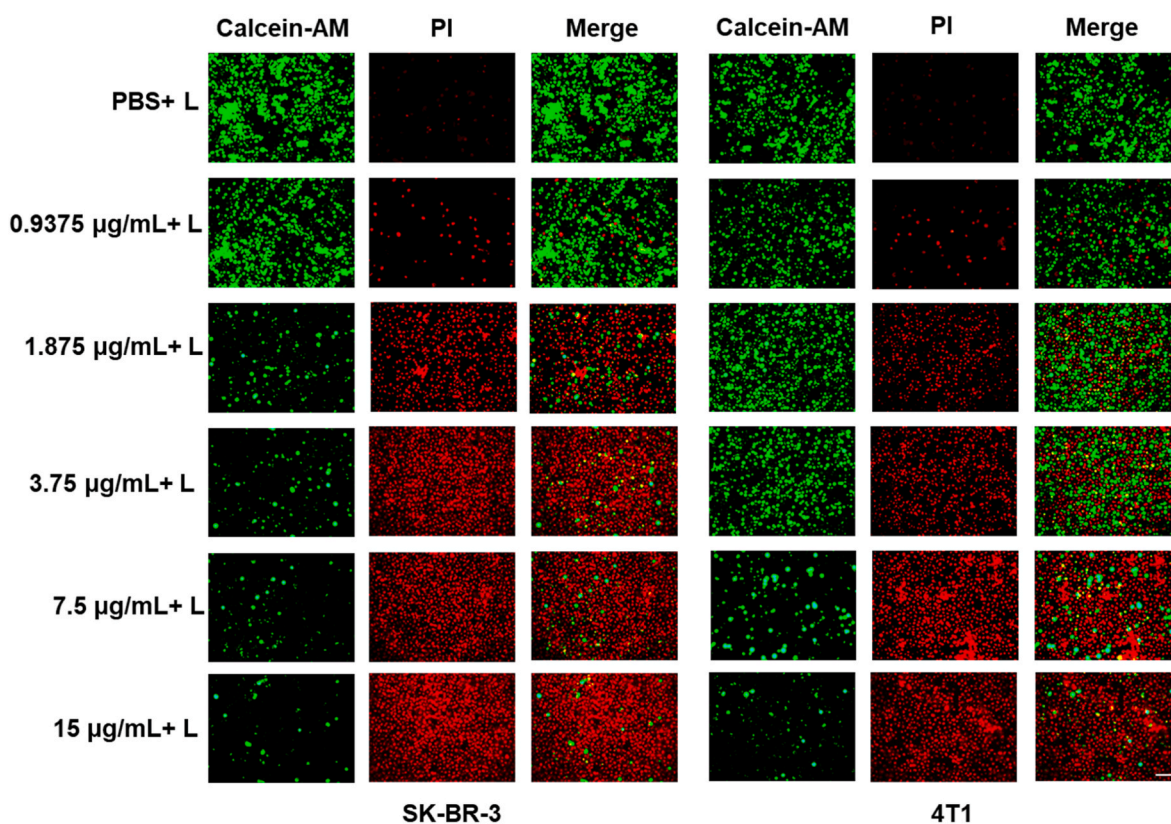
Fig. 4. Calcein-AM/PI dual staining of SK-BR-3 and 4T1 cells cocultured with different concentrations of BP-PEG-MTO-Tmab for 6 h and irradiated with an 808 nm laser (+L) at the power density of 1.0 W/cm^2 for 10 min (scale bar = 100 μm).

displayed excellent photothermal stability after five laser on/off cycles (Fig. 2f). These results indicated that the complexes could be as a great PTT agent owing to their excellent photothermal efficacy and stability.

3.2. In vitro cytotoxicity

We used CCK-8 assay to evaluate the cytotoxicity of BP-PEG-Tmab, BP-PEG-MTO-Tmab, and free MTO. As shown in Fig. 3a and b, the nanocarrier of BP-PEG-Tmab displayed no obvious cytotoxicity in both SK-BR-3 and 4T1, because the viability of SK-BR-3 and 4T1 cells were both higher than 90% at the given BP concentrations. It indicated that BP-PEG-Tmab had satisfactory biocompatibility *in vitro*. Whereas, BP-PEG-MTO-Tmab and free MTO can effectively destroy both tumor

cells. For SK-BR-3 cancer cells, the IC50 values of BP-PEG-MTO-Tmab and free MTO were 13.13 μg/mL and 7.21 μg/mL, respectively (Fig. 3a). Similarly, for 4T1 cancer cells, the IC50 values of BP-PEG-MTO-Tmab and free MTO were 19.22 μg/mL and 7.99 μg/mL, respectively (Fig. 3b). Notably, the cytotoxicity of BP-PEG-MTO-Tmab was lower than that of free MTO at the same drug concentration either in SK-BR-3 cells or 4T1 cells. The reason may be that part of the BP-PEG-MTO-Tmab complexes stuck to cell surface that was difficult to be cleaned thoroughly, and 2D BP has certain light absorption at 450 nm, causing it to show high cell viability. In addition, the IC50 value of BP-PEG-MTO-Tmab complexes to SK-BR-3 cells was a little lower than that to 4T1 cells, indicating that the complexes exerted a targeting effect through HER2-overexpressed receptors.
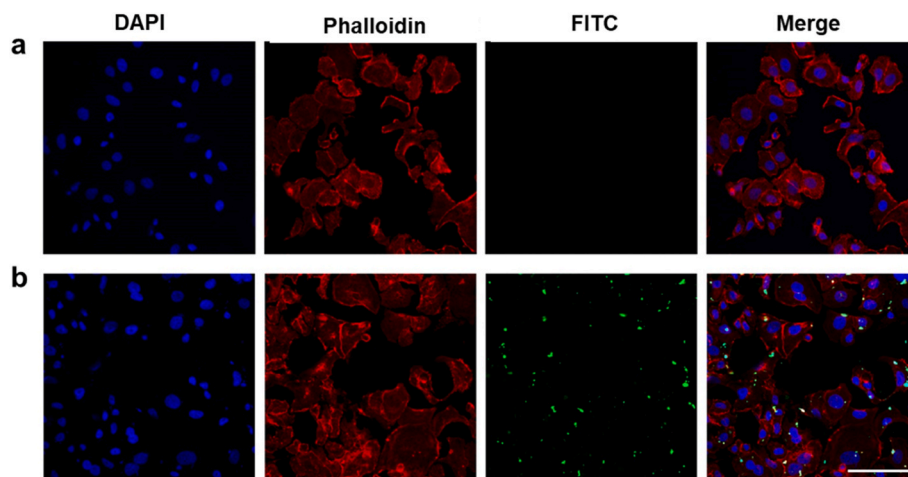

Fig. 5. Confocal images of BP-PEG-FITC-MTO (a) and BP-PEG-FITC-MTO-Tmab (b) cocultured with HER2-positive SK-BR-3 cells for 1 h (scale bar = 100 μm).
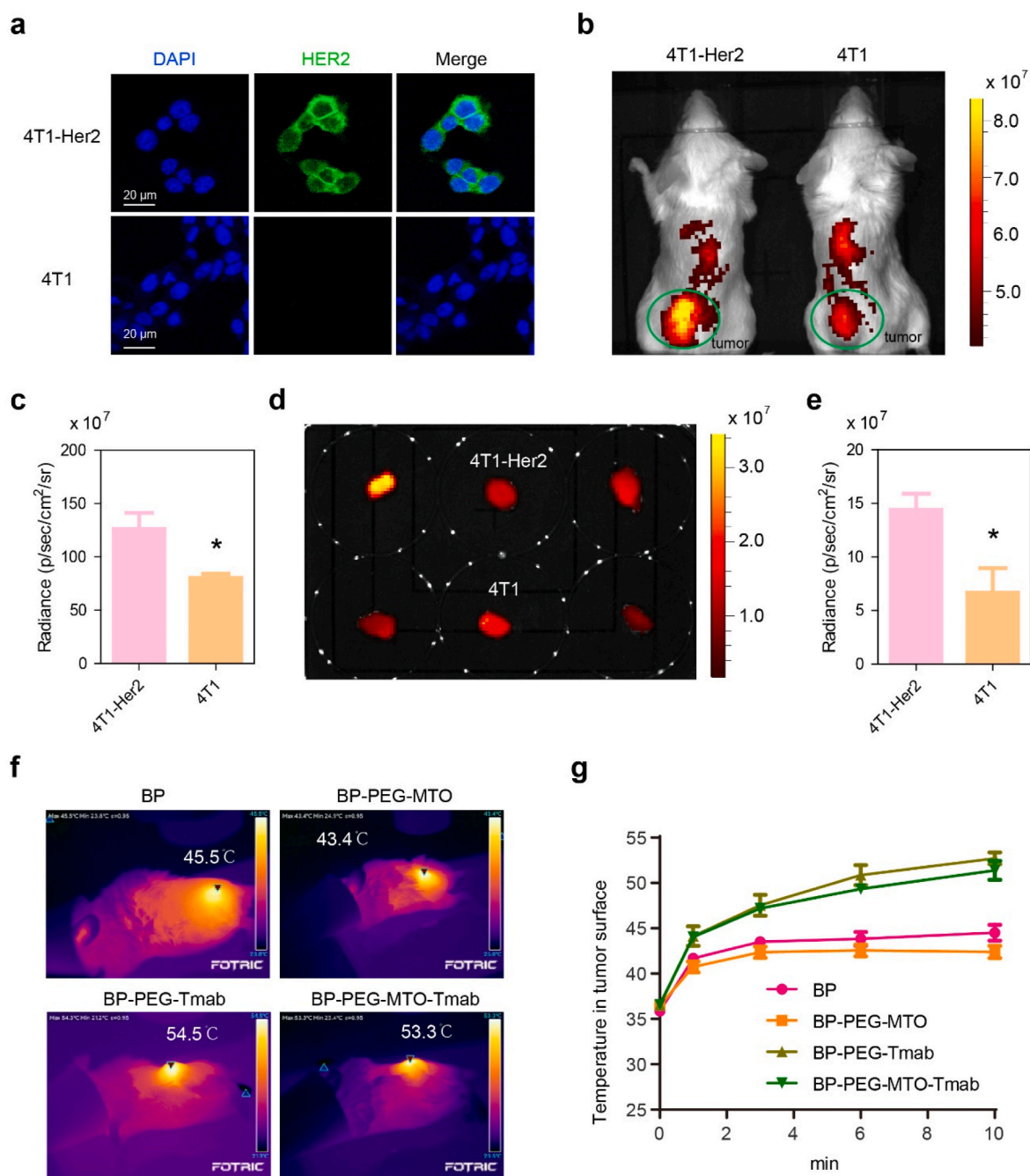
Fig. 6. (a) Immunofluorescence staining of HER-2 (green signal) and DAPI (blue signal) in 4T1 control cells and HER-2 overexpressing 4T1-Her2 cells, scale bars = 20 μm. (b–c) Representative fluorescent images of HER-2 positive 4T1-Her2 tumors (left, n = 3) and HER-2 negative 4T1 tumors (right, n = 3) visualized from IVIS Kinetic 24 h after intravenous injection with BP-ICG-Tmab. The ICG fluorescence intensity was enriched in 4T1-Her2 tumors than 4T1 group (*p < 0.05). (d–e) Comparable pattern of tumors ICG fluorescence between 4T1-Her2 (upper panel) and 4T1 (lower panel) tumors *ex vivo* (*p < 0.05). (f–g) The *in vivo* thermographic surveillance of photothermal heating in mice bearing 4T1-Her2 tumors after intravenous injection with/without Tmab nanoparticles (BP, BP-PEG-MTO, BP-PEG-Tmab, BP-PEG-MTO-Tmab; n = 5 for each group) and irradiation for 10 min using an 808 nm laser at 1.0 W/cm².

3.3. In vitro PTT

In vitro PTT of BP-PEG-MTO-Tmab complexes was further investigated. As shown in Fig. 3c, the complexes effectively killed both types of tumor cells under 808 nm laser (1.0 W/cm²) irradiation. When the MTO concentration of BP-PEG-MTO-Tmab was up to 15 μg/mL, the maximum temperature of the cells/complexes increased to higher 70 °C, leading to an excellent PTT effect *in vitro*. However, at low concentrations, the complexes treated HER2-positive SK-BR-3 cells were more severely damaged than that of HER2-negative 4T1 cells, such as causing 79% cell

death even at MTO concentration of 1.875 μg/mL, whereas 43% cell death for 4T1 cells. The reason is that BP-PEG-MTO-Tmab complexes were able to cluster around SK-BR-3 cells through a targeting effect and effectively taken up by the cells (Fig. S4).

These results were further confirmed by calcein-AM/PI dual staining assay. As shown in Fig. 4, under laser irradiation, the more treated cells died as the concentration increased, which was visible in PI-associated red fluorescence. Furthermore, the SK-BR-3 cells treated by the complexes had more dead cells than 4T1 cells at the same concentration (Fig. 4). It was suggested that BP-PEG-MTO-Tmab complexes had a
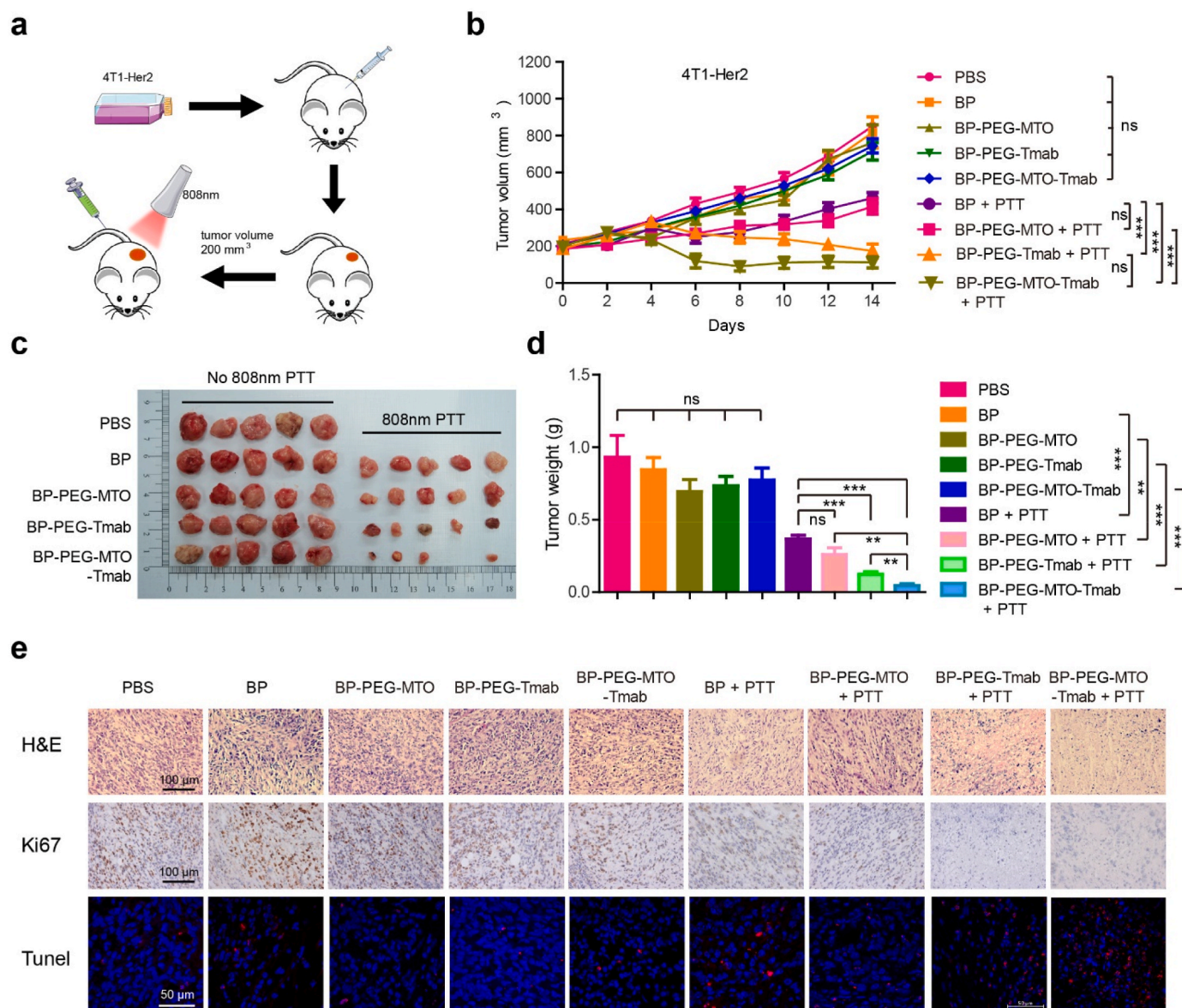
Fig. 7. (a) Schematic representation of 4T1-Her2 tumor ectopic implantation model and phototherapy in mice. (b) Variation in tumor volume of mice after intravenous injection of PBS, BP, BP-PEG-MTO, BP-PEG-Tmab, BP-PEG-MTO-Tmab with/without 808 nm laser irradiation (1.0 W/cm^2) for 10 min at an initial stage (n = 5 per group, ***p < 0.001, ns = not significant). (c–d) Representative images of tumor volume and quantified data of tumor mass (**p < 0.01, ***p < 0.001). (e) Representative images of H&E staining (scale bars = 100 μm), immunohistochemical staining for Ki67 (scale bars = 100 μm), and TUNEL staining (scale bars = 50 μm) in tumor tissue.

stronger targeted PTT effect on HER2-positive cells.

3.4. In vitro targeting specificity

To further explore *in vitro* targeting specificity of BP-PEG-MTO-Tmab complexes, we used FITC modified the complexes for CLSM imaging. SK-BR-3 cells treated with Tmab-targeted BP-PEG-FITC-MTO-Tmab displayed obvious FITC green fluorescence, while nontargeted BP-PEG-FITC-MTO showed a small amount of FITC green fluorescence (Fig. 5). Quantification of fluorescence signal confirmed that HER2-targeted BP-PEG-FITC-MTO-Tmab showed a much higher FITC fluorescence signal in SK-BR-3 cells than nontargeted BP-PEG-FITC-MTO (Fig. S5). The results indicated that the BP-PEG-MTO-Tmab complexes had satisfactoy targeting specificity to cancer cells overexpressing HER2 receptors.

3.5. HER2-targeted accumulation and photothermal effect of BP-PEG-MTO-Tmab in vivo

Strategies aimed at improving the delivery of photothermal agents to tumor tissues *in vivo* have gained considerable attention due to their potential to enhance the selectivity and efficacy of PTT simultaneously [12]. Many previous studies have utilized the method of intratumoral injection of 2D BP for local PTT of tumors [34,51]. However, this often results in the uneven distribution of photothermal agents within the tumor tissue, thereby affecting the overall effectiveness of tumor PTT. Although the use of intravenous administration and the tumor EPR effect can lead to relatively uniform accumulation of 2D BP in tumors, however, the validity of the EPR effect in human tumors, and whether it is as significant as it is in rapidly growing tumors in murine models, is uncertain [55,56].

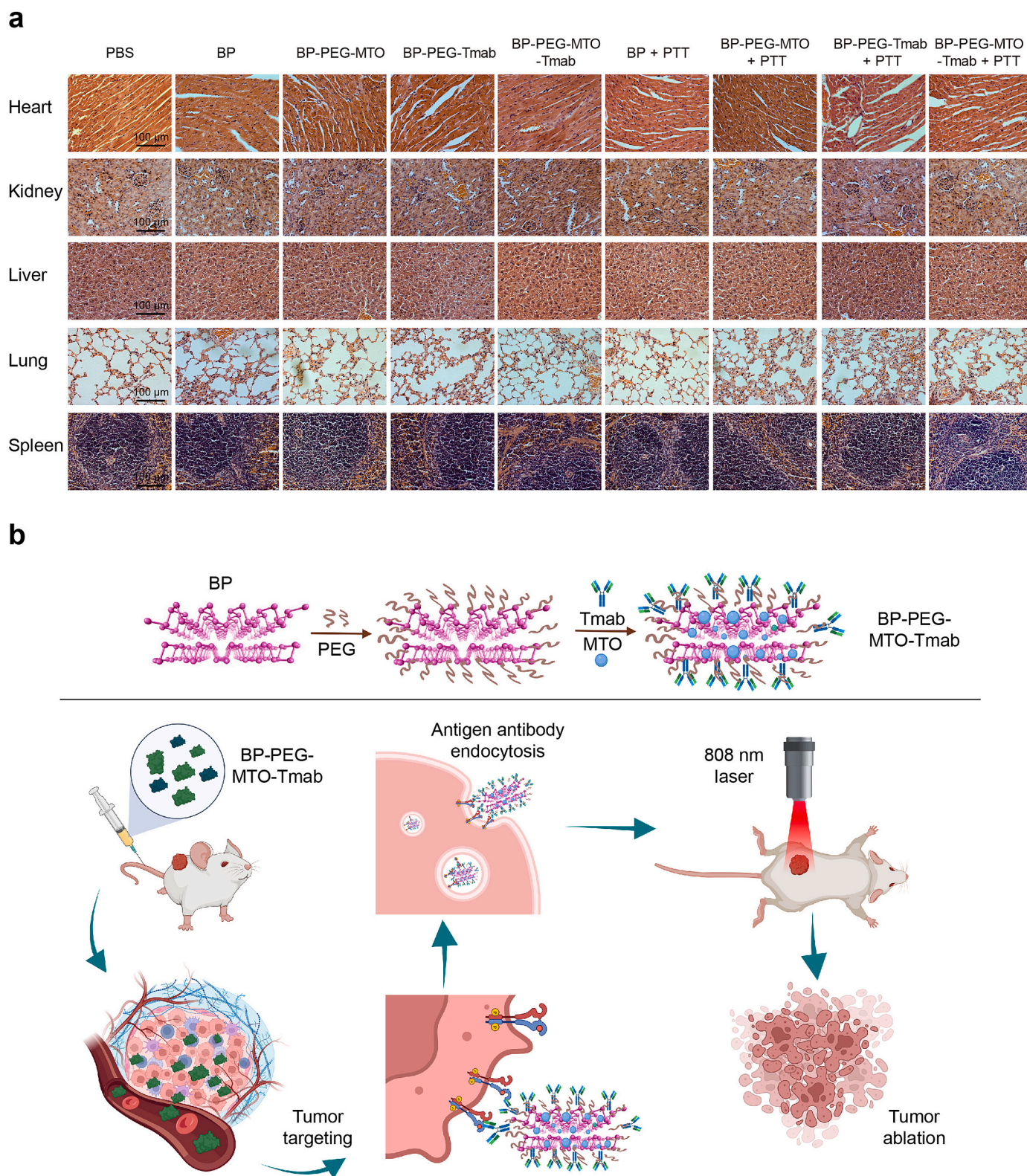To examine the distribution of the BP-PEG-MTO-Tmab *in vivo*, we

Fig. 8. (a) Representative images of H&E staining of organs (heart, kidney, liver, lung, and spleen) tissue in the xenograft models after different treatments. (b) Schematic model for BP-PEG-MTO-Tmab in targeted PTT in HER2-positive breast cancer.

generated ectopic xenograft tumor model with HER2-positive 4T1-Her2 cells and HER2-negative 4T1 cells (Fig. 6a) in the dorsum of mice. Furthermore, we conjugated BP-Tmab with indocyanine green (ICG), the most commonly used FDA-approved agent for clinical optical imaging, and visualized the hybrid nanodrug biodistribution in mouse

xenograft model. The ICG fluorescence intensity was visualized by using the IVIS Kinetic system 24 h after intravenous injection of 1 mg/kg of ICG-labeled BP-Tmab. We found that the fluorescence in HER2-positive 4T1-Her2 tumors were significantly stronger than the HER2-negative 4T1 tumors (Fig. 6b). Ex vivo ICG signal analysis in tumors confirmed

that significantly higher fluorescent signal of BP-ICG-Tmab enriched in 4T1-Her2 tumors compared with the 4T1 tumors. These suggested that Tmab-modified BP showed a HER2-targeted accumulation in tumors.

2D BP provided a high efficiency for tumor PTT [34,51,57]. Next, we determined the photothermal property of BP, BP-PEG-MTO, BP-PEG-T-mab, and BP-PEG-MTO-Tmab *in vivo*. 24 h after intravenous injection of BP and BP hybrid nanodrug (150 μL, 1 mg/mL of BP), mice were anesthetized and tumors were irradiated with an 808 nm laser (1.0 W/cm^2) for 10 min. Temperature monitoring data showed that temperature in the 4T1-Her2 tumors treated with BP-Tmab and BP-PEG-MTO-Tmab increased to nearly 54 °C (54.5 °C and 53.3 °C respectively), while temperature tumors in BP and BP-PEG-MTO groups kept around 45 °C (45.5 °C and 43.4 °C respectively) during the laser irradiation. Exposure of tissues to temperatures within the range of 42–46 °C for 10 min led to the necrosis of cells. Additionally, at temperatures between 46 and 52 °C, cell death occurs rapidly due to microvascular thrombosis and ischemia [58]. These results suggested that the conjugation of Tmab could improve the distribution of BP in HER2-positive tumors, and dramatically increase the photothermal therapeutic efficacy *in vivo*.

3.6. In vivo antitumor studies

For HER-2 positive breast cancer patients, HER2-specific antibody-drug conjugate showed a significant improvement in eliminating tumor lesion and overall survival [59]. Strategies for coupling BP and chemotherapeutics to HER2-targeted antibodies may enhance the accumulation of BP and chemotherapeutics within the tumor tissues specifically and facilitate antigen-antibody endocytosis. After irradiating with an 808 nm laser, 2D BP in tumor cells rapidly produced enough thermal energy to kill cells and promoted the release of chemotherapeutics within tumor cells, which caused cytotoxic effect and bystander effect. We next assessed *in vivo* antitumor efficacy of Tmab-based BP in HER2-positive breast cancer. Balb/c mice orthotopically implanted with 4T1-Her2 cells were randomly divided into 9 groups after the tumor volume reached about 100 mm^3 and were intravenous injected with BP hybrid nanodrugs (150 μL, 1 mg/mL of BP) by irradiation with an 808 nm laser (1.0 W/cm^2) for once (Fig. 7a). Mice treated with PBS or BP hybrid nanodrugs without laser irradiation were included as control groups. With one dose of BP hybrid nanodrugs injection without PTT treatment had little effect on tumor growth compared with the PBS control group. It demonstrated that a single low dose of Tmab or MTO chemotherapy did not show any tumor suppression effect. The tumor growth in BP and BP-PEG-MTO groups with PPT suppressed significantly compared with groups without PPT. Meanwhile, tumors in BP-PEG-Tmab and BP-PEG-MTO-Tmab groups with laser irradiation were suppressed and shrunk obviously, and tumor recurrence was dramatically delayed compared with BP and BP-PEG-MTO groups after PTT. Moreover, tumors treated with BP-PEG-MTO-Tmab + PTT showed the most obvious deceleration of tumor growth, which suggested that even the combination of one single low dose of MTO may cause lethal toxicity after tumor cells suffering effective photothermal damage (Fig. 7b–d). As shown in Fig. 7d, the tumor volume in the BP-PEG-MTO-Tmab + PTT group was diminished more significantly than that in the BP-PEG-MTO + PTT group and BP-Tmab + PTT group, suggesting that the combined use of Tmab and MTO had a more pronounced killing effect on the tumor in the presence of PTT. Additionally, the tumor volume in the BP-PEG-MTO-Tamb + PTT group was also diminished more significantly than that in BP-PEG-MTO-Tamb without laser irradiation. These are consistent with our intended design of the targeted chemo-photothermal nanodrug. Therefore, at the animal experiment level, it demonstrated that the BP-PEG-MTO-Tmab nanodrug exhibited a synergistic antitumor efficacy.

In addition, to determine the proliferation potential or cell apoptosis of tumors with different BP hybrid nanodrug treatments, tumor tissue from different groups of mice were collected at 14 days post treatment. H&E, immunohistochemical Ki67 staining, and terminal deoxynucleotidyl transferase dUTP nick-end labeling (TUNEL) assay were performed to analyze the therapeutic effect at the pathological level. H&E staining showed that tumors treated with PTT induced necrotic cell death. Particularly, we found a massive granulation with chronic inflammatory and lymphocyte infiltration change in tumor tissue BP-PEG-Tmab and BP-PEG-MTO-Tmab groups treated with PTT (Fig. 7e upper panel). The results of Ki67 staining and TUNEL assay demonstrated that the expressions of Ki-67 were obviously reduced while the apoptosis signals were increased in tumor tissue of BP-Tmab and BP-PEG-MTO-Tmab groups with PTT, and mild decrease of Ki-67 expressions and a few apoptosis signals were observed in the BP and BP-PEG-MTO groups with PTT, which was consistent with the H&E pathological changes (Fig. 7e).

To further investigate the biological safety of various BP hybrid nanodrug treatments, major organs including heart, kidney, liver, lung, and spleen were corrected and performed H&E staining. Obvious pathological changes of damage or inflammation were not observed compared with the PBS control group (Fig. 8a). In the course of receiving treatment, the body weights of mice were well maintained, indicating the treatment achieved with good tolerance (Fig. S6). Thus, the HER-2 targeted BP-PEG-MTO-Tmab had high levels of light absorption at the treatment wavelength, high photothermal conversion efficiency and photostability, and good biocompatibility. Fig. 8b showed the schematic model for BP-PEG-MTO-Tmab in targeted PTT in HER2-positive breast cancer.

4. Conclusions

In summary, an optimal framework for clinical photothermal therapy of breast cancer should be established by taking into comprehensive account factors such as molecular cancer type, tumor heterogeneity, and biological properties, etc. In this study, we developed BP-PEG-MTO-Tmab complexes as safe, tumor active targeting, and highly effective tumor ablation for HER2-positive breast cancer. In comparison to existing photothermal therapy, chemotherapy, or targeted therapy approaches, our novel approach utilizing HER2-targeted photothermal tumor ablation with 2D BP in combination with a chemotherapeutic drug exhibits the potential to address multiple pivotal challenges encountered in the comprehensive treatment of breast cancer.

Declaration of competing interest

The authors declare that they have no known competing financial interests or personal relationships that could have appeared to influence the work reported in this paper.

Data availability

Data will be made available on request.

Appendix A. Supplementary data

Supplementary data to this article can be found online at https://doi.org/10.1016/j.mtbio.2023.100812.

References

[1] H. Sung, J. Ferlay, R.L. Siegel, M. Laversanne, I. Soerjomataram, A. Jemal, F. Bray, Global cancer statistics 2020: GLOBOCAN estimates of incidence and mortality worldwide for 36 cancers in 185 countries, Ca-Cancer J. Clin. 71 (3) (2021) 209–249, https://doi.org/10.3322/caac.21660.

[2] H. Kawaji, M. Kubo, N. Yamashita, H. Yamamoto, M. Kai, A. Kajihara, M. Yamada, K. Kurata, K. Kaneshiro, Y. Harada, S. Hayashi, A. Shimazaki, H. Mori, S. Akiyoshi, E. Oki, Y. Oda, E. Baba, M. Mori, M. Nakamura, Comprehensive molecular profiling broadens treatment options for breast cancer patients, Cancer Med. 10 (2) (2021) 529–539, https://doi.org/10.1002/cam4.3619.

[3] C. Denkert, F. Seither, A. Schneeweiss, T. Link, J.U. Blohmer, M. Just, P. Wimberger, A. Forberger, H. Tesch, C. Jackisch, S. Schmatloch, M. Reinisch, E. F. Solomayer, W.D. Schmitt, C. Hanusch, P.A. Fasching, K. Lubbe, C. Solbach, J. Huober, K. Rhiem, F. Marme, T. Reimer, M. Schmidt, B.V. Sinn, W. Janni, E. Stickeler, L. Michel, O. Stotzer, E. Hahnen, J. Furlanetto, S. Seiler, V. Nekljudova, M. Untch, S. Loibl, Clinical and molecular characteristics of HER2-low-positive breast cancer: pooled analysis of individual patient data from four prospective, neoadjuvant clinical trials, Lancet Oncol. 22 (8) (2021) 1151–1161, https://doi.org/10.1016/s1470-2045(21)00301-6.

[4] K.A. Cronin, L.C. Harlan, K.W. Dodd, J.S. Abrams, R. Ballard-Barbash, Population-based estimate of the prevalence of HER-2 positive breast cancer tumors for early stage patients in the US, Cancer Invest. 28 (9) (2010) 963–968, https://doi.org/10.3109/07357907.2010.496759.

[5] J. Kreutzfeldt, B. Rozeboom, N. Dey, P. De, The trastuzumab era: current and upcoming targeted HER2+ breast cancer therapies, Am. J. Cancer Res. 10 (4) (2020) 1045–1067.

[6] S. Vivekanandhan, K.L. Knutson, Resistance to trastuzumab, Cancers 14 (20) (2022) 5115, https://doi.org/10.3390/cancers14205115.

[7] K. Tamura, J. Tsurutani, S. Takahashi, H. Iwata, I.E. Krop, C. Redfern, Y. Sagara, T. Doi, H. Park, R.K. Murthy, R.A. Redman, T. Jikoh, C. Lee, M. Sugihara, J. Shahidi, A. Yver, S. Modi, Trastuzumab deruxtecan (DS-8201a) in patients with advanced HER2-positive breast cancer previously treated with trastuzumab emtansine: a dose-expansion, phase 1 study, Lancet Oncol. 20 (6) (2019) 816–826, https://doi.org/10.1016/s1470-2045(19)30097-x.

[8] S. Modi, W. Jacot, T. Yamashita, J. Sohn, M. Vidal, E. Tokunaga, J. Tsurutani, N. T. Ueno, A. Prat, Y.S. Chae, K.S. Lee, N. Niikura, Y.H. Park, B. Xu, X. Wang, M. Gil-Gil, W. Li, J.-Y. Pierga, S.-A. Im, H.C.F. Moore, H.S. Rugo, R. Yerushalmi, F. Zagouri, A. Gombos, S.-B. Kim, Q. Liu, T. Luo, C. Saura, P. Schmid, T. Sun, D. Gambhire, L. Yung, Y. Wang, J. Singh, P. Vitazka, G. Meinhardt, N. Harbeck, D. A. Cameron, Trastuzumab deruxtecan in previously treated HER2-low advanced breast cancer, N. Engl. J. Med. 387 (1) (2022) 9–20, https://doi.org/10.1056/NEJMoa2203690.

[9] P. Narayan, C.L. Osgood, H. Singh, H.-J. Chiu, T.K. Ricks, E.C.Y. Chow, J. Qiu, P. Song, J. Yu, F. Namuswe, S. Hou, W.F. Pierce, K.B. Goldberg, S. Tang, L. Amiri-Kordestani, M.R. Theoret, R. Pazdur, J.A. Beaver, FDA approval summary: fam-trastuzumab deruxtecan-nxki for the treatment of unresectable or metastatic HER2-positive breast cancer, Clin. Cancer Res. 27 (16) (2021) 4478–4485, https://doi.org/10.1158/1078-0432.ccr-20-4557.

[10] Z. Xu, D. Guo, Z. Jiang, R. Tong, P. Jiang, L. Bai, L. Chen, Y. Zhu, C. Guo, J. Shi, D. Yu, Novel HER2-targeting antibody-drug conjugates of trastuzumab beyond T-DM1 in breast cancer: trastuzumab deruxtecan(DS-8201a) and (Vic-)Trastuzumab duocarmazine (SYD985), Eur. J. Med. Chem. 183 (2019) 111682, https://doi.org/10.1016/j.ejmech.2019.111682.

[11] J. Cortes, S.B. Kim, W.P. Chung, S.A. Im, Y.H. Park, R. Hegg, M.H. Kim, L.M. Tseng, V. Petry, C.F. Chung, H. Iwata, E. Hamilton, G. Curigliano, B. Xu, C.S. Huang, J. H. Kim, J.W.Y. Chiu, J.L. Pedrini, C. Lee, Y. Liu, J. Cathcart, E. Bako, S. Verma, S. A. Hurvitz, D.E.-B.T. Investigators, Trastuzumab deruxtecan versus trastuzumab emtansine for breast cancer, N. Engl. J. Med. 386 (12) (2022) 1143–1154, https://doi.org/10.1056/NEJMoa2115022.

[12] X. Li, J.F. Lovell, J. Yoon, X. Chen, Clinical development and potential of photothermal and photodynamic therapies for cancer, Nat. Rev. Clin. Oncol. 17 (11) (2020) 657–674, https://doi.org/10.1038/s41571-020-0410-2.

[13] W. He, Y. Jiang, Q. Li, D. Zhang, Z. Li, Y. Luan, A versatile strategy to create an active tumor-targeted chemo-photothermal therapy nanoplatform: a case of an IR-780 derivative co-assembled with camptothecin prodrug, Acta Biomater. 84 (2019) 356–366, https://doi.org/10.1016/j.actbio.2018.11.049.

[14] D. Yu, Y. Wang, J. Chen, S. Liu, S. Deng, C. Liu, I. McCulloch, W. Yue, D. Cheng, Co-delivery of NIR-II semiconducting polymer and pH-sensitive doxorubicin-conjugated prodrug for photothermal/chemotherapy, Acta Biomater. 137 (2022) 238–251, https://doi.org/10.1016/j.actbio.2021.10.009.

[15] J.X. Liu, C. Zhao, W.R. Chen, B.Q. Zhou, Recent progress in two-dimensional nanomaterials for cancer theranostics, Coord. Chem. Rev. 469 (2022) 214654, https://doi.org/10.1016/j.ccr.2022.214654.

[16] M. Wang, J. Song, F.F. Zhou, A.R. Hoover, C. Murray, B.Q. Zhou, L. Wang, J.L. Qu, W.R. Chen, NIR-triggered phototherapy and immunotherapy via an antigen-capturing nanoplatform for metastatic cancer treatment, Adv. Sci. 6 (10) (2019), 1802157, https://doi.org/10.1002/advs.201802157.

[17] B.Q. Zhou, J.X. Liu, M.A. Lin, J.Y. Zhu, W.R. Chen, Recent advances in immunotherapy, immunoadjuvant, and nanomaterial-based combination immunotherapy, Coord. Chem. Rev. 442 (2021) 214009, https://doi.org/10.1016/j.ccr.2021.214009.

[18] B.Q. Zhou, J.X. Liu, L. Wang, M. Wang, C. Zhao, H.Y. Lin, Y.K. Liang, R.A. Towner, W.R. Chen, Iron oxide nanoparticles as a drug carrier reduce host immunosuppression for enhanced chemotherapy, Nanoscale 14 (12) (2022) 4588–4594, https://doi.org/10.1039/d1nr07750c.

[19] B.Q. Zhou, Q. Wu, M. Wang, A. Hoover, X. Wang, F.F. Zhou, R.A. Towner, N. Smith, D. Saunders, J. Song, J.L. Qu, W.R. Chen, Immunologically modified MnFe2O4 nanoparticles to synergize photothermal therapy and immunotherapy for cancer treatment, Chem. Eng. J. 396 (2020), 125239, https://doi.org/10.1016/j.cej.2020.125239.

[20] P. Huang, Y. Yang, W.Y. Wang, Z.M. Li, N.S. Gao, H.Z. Chen, X.W. Zeng, Self-driven nanoprodrug platform with enhanced ferroptosis for synergistic photothermal-Ido immunotherapy, Biomaterials 299 (2023), 122157, https://doi.org/10.1016/j.biomaterials.2023.122157.

[21] S.P. Feng, J.Y. Lu, K.L. Wang, D.H. Di, Z.N. Shi, Q.F. Zhao, S.L. Wang, Advances in smart mesoporous carbon nanoplatforms for photothermal-enhanced synergistic cancer therapy, Chem. Eng. J. 435 (2022) 134886, https://doi.org/10.1016/j.cej.2022.134886.

[22] Q.Q. Xu, Y.Q. Yang, J.Y. Lu, Y.Z. Lin, S.P. Feng, X.Y. Luo, D.H. Di, S.L. Wang, Q. F. Zhao, Recent trends of mesoporous silica-based nanoplatforms for nanodynamic therapies, Coord. Chem. Rev. 469 (2022) 214687, https://doi.org/10.1016/j.ccr.2022.214687.

[23] H.W. Xu, Y. Zhang, H.T. Zhang, Y.R. Zhang, Q.Q. Xu, J.Y. Lu, S.P. Feng, X.Y. Luo, S. L. Wang, Q.F. Zhao, Smart polydopamine-based nanoplatforms for biomedical applications: state-of-art and further perspectives, Coord. Chem. Rev. 488 (2023), 215153, https://doi.org/10.1016/j.ccr.2023.215153.

[24] M. Pumera, Z. Sofer, 2D monoelemental arsenene, antimonene, and bismuthene: beyond black phosphorus, Adv. Mater. 29 (21) (2017), 1605299, https://doi.org/10.1002/adma.201605299.

[25] J. Pang, A. Bachmatiuk, Y. Yin, B. Trzebicka, L. Zhao, L. Fu, R.G. Mendes, T. Gemming, Z. Liu, M.H. Rummeli, Applications of phosphorene and black phosphorus in energy conversion and storage devices, Adv. Energy Mater. 8 (8) (2018), 1702093, https://doi.org/10.1002/aenm.201702093.

[26] F. Xia, H. Wang, Y. Jia, Rediscovering black phosphorus as an anisotropic layered material for optoelectronics and electronics, Nat. Commun. 5 (2014) 4458, https://doi.org/10.1038/ncomms5458.

[27] H. Liu, Y. Du, Y. Deng, P.D. Ye, Semiconducting black phosphorus: synthesis, transport properties and electronic applications, Chem. Soc. Rev. 44 (9) (2015) 2732–2743, https://doi.org/10.1039/c4cs00257a.

[28] F.R. Fan, R.X. Wang, H. Zhang, W.Z. Wu, Emerging beyond-graphene elemental 2D materials for energy and catalysis applications, Chem. Soc. Rev. 50 (19) (2021) 10983–11031, https://doi.org/10.1039/c9cs00821g.

[29] Y. Wang, L. Wang, X. Zhang, X.J. Liang, Y.Y. Feng, W. Feng, Two-dimensional nanomaterials with engineered bandgap: synthesis, properties, applications, Nano Today 37 (2021), 101059, https://doi.org/10.1016/j.nantod.2020.101059.

[30] Y. Liu, M. Yang, J. Lu, Y. Liu, H. Liu, E. Zhang, W. Fu, J. Wang, Z. Hu, J. Yin, G. Eda, S. Wang, J. Yi, A. Vinu, K.P. Loh, Tuning photoresponse of graphene-black phosphorus heterostructure by electrostatic gating and photo-induced doping, Chin. Chem. Lett. 33 (1) (2022) 368–373, https://doi.org/10.1016/j.cclet.2021.06.079.

[31] A. Castellanos-Gomez, Black phosphorus: narrow gap, wide applications, J. Phys. Chem. Lett. 6 (21) (2015) 4280–4291, https://doi.org/10.1021/acs.jpclett.5b01686.

[32] Z. Sun, H. Xie, S. Tang, X.F. Yu, Z. Guo, J. Shao, H. Zhang, H. Huang, H. Wang, P. K. Chu, Ultrasmall black phosphorus quantum dots: synthesis and use as photothermal agents, Angew. Chem., Int. Ed. 54 (39) (2015) 11526–11530.

[33] J.K. Zeng, X.W. Geng, Y.F. Tang, Z.C. Xiong, Y.J. Zhu, X.S. Chen, Flexible photothermal biopaper comprising Cu2+-doped ultralong hydroxyapatite nanowires and black phosphorus nanosheets for accelerated healing of infected wound, Chem. Eng. J. 437 (2022) 135347, https://doi.org/10.1016/j.cej.2022.135347.

[34] W. Tao, X. Zhu, X. Yu, X. Zeng, Q. Xiao, X. Zhang, X. Ji, X. Wang, J. Shi, H. Zhang, L. Mei, Black phosphorus nanosheets as a robust delivery platform for cancer theranostics, Adv. Mater. 29 (1) (2017), 1603276, https://doi.org/10.1002/adma.201603276.

[35] W.F. Zeng, Z. Li, H.Z. Chen, X.W. Zeng, L. Mei, An optimal portfolio of photothermal combined immunotherapy, Cell Rep. Phys. Sci. 3 (6) (2022), 100898, https://doi.org/10.1016/j.xcrp.2022.100898.

[36] M.T. Ou, C.C. Lin, Y. Wang, Y.T. Lu, W.Y. Wang, Z.M. Li, W.W. Zeng, X.W. Zeng, X. Y. Ji, L. Mei, Heterojunction engineered bioactive chlorella for cascade promoted cancer therapy, J. Contr. Release 345 (2022) 755–769, https://doi.org/10.1016/j.jconrel.2022.03.059.

[37] X.Y. Ye, X. Liang, Q. Chen, Q.W. Miao, X.L. Chen, X.D. Zhang, L. Mei, Surgical tumor-derived personalized photothermal vaccine formulation for cancer immunotherapy, ACS Nano 13 (3) (2019) 2956–2968, https://doi.org/10.1021/acsnano.8b07371.

[38] Z. Li, Y. Yu, W. Zeng, F. Ding, D. Zhang, W. Cheng, M. Wang, H. Chen, G. Pan, L. Mei, X. Zeng, N. Gao, Mussel-inspired ligand clicking and ion coordination on 2D black phosphorus for cancer multimodal imaging and therapy, Small 18 (26) (2022) 2201803, https://doi.org/10.1002/smll.202201803.

[39] J. Qi, Y. Xiong, K. Cheng, Q. Huang, J. Cao, F. He, L. Mei, G. Liu, W. Deng, Heterobifunctional PEG-grafted black phosphorus quantum dots: "Three-in-One" nano-platforms for mitochondria-targeted photothermal cancer therapy, Asian J. Pharm. Sci. 16 (2) (2021) 222–235, https://doi.org/10.1016/j.ajps.2020.09.001.

[40] N. Gao, L. Mei, Black phosphorus-based nano-drug delivery systems for cancer treatment: opportunities and challenges, Asian J. Pharm. Sci. 16 (1) (2021) 1–3, https://doi.org/10.1016/j.ajps.2020.03.004.

[41] M. Qiu, D. Wang, W.Y. Liang, L.P. Liu, Y. Zhang, X. Chen, D.K. Sang, C.Y. Xing, Z. J. Li, B.Q. Dong, F. Xing, D.Y. Fan, S.Y. Bao, H. Zhang, Y.H. Cao, Novel concept of the smart NIR-light-controlled drug release of black phosphorus nanostructure for

cancer therapy, Proc. Natl. Acad. Sci. U. S. A. 115 (3) (2018) 501–506, https://doi.org/10.1073/pnas.1714421115.

[42] G. Qu, T. Xia, W. Zhou, X. Zhang, H. Zhang, L. Hu, J. Shi, X.-F. Yu, G. Jiang, Property-activity relationship of black phosphorus at the nano-bio interface: from molecules to organisms, Chem. Rev. 120 (4) (2020) 2288–2346, https://doi.org/10.1021/acs.chemrev.9b00445.

[43] T. Chen, W.W. Zeng, C.J. Tie, M. Yu, H.S. Hao, Y. Deng, Q.Q. Li, H.R. Zheng, M.Y. Wu, L. Mei, Engineered gold/black phosphorus nanoplatforms with remodeling tumor microenvironment for sonoactivated catalytic tumor theranostics, Bioact. Mater. 10 (2022) 515–525, https://doi.org/10.1016/j.bioactmat.2021.09.016.

[44] C.C. Jia, F. Zhang, J.M. Lin, L.W. Feng, T.T. Wang, Y. Feng, F. Yuan, Y. Mai, X.W. Zeng, Q. Zhang, Black phosphorus-Au-thiosugar nanosheets mediated photothermal induced anti-tumor effect enhancement by promoting infiltration of NK cells in hepatocellular carcinoma, J. Nanobiotechnol. 20 (1) (2022) 90, https://doi.org/10.1186/s12951-022-01286-z.

[45] J. Kang, J.D. Wood, S.A. Wells, J.H. Lee, X.L. Liu, K.S. Chen, M.C. Hersam, Solvent exfoliation of electronic-grade, two-dimensional black phosphorus, ACS Nano 9 (4) (2015) 3596–3604, https://doi.org/10.1021/acsnano.5b01143.

[46] H. Wang, X.Z. Yang, W. Shao, S.C. Chen, J.F. Xie, X.D. Zhang, J. Wang, Y. Xie, Ultrathin black phosphorus nanosheets for efficient singlet oxygen generation, J. Am. Chem. Soc. 137 (35) (2015) 11376–11382, https://doi.org/10.1021/jacs.5b06025.

[47] Y. Yi, X.F. Yu, W.H. Zhou, J.H. Wang, P.K. Chu, Two-dimensional black phosphonts: synthesis, modification, properties, and applications, Mater. Sci. Eng., R 120 (2017) 1–33, https://doi.org/10.1016/j.mser.2017.08.001.

[48] X.W. Zeng, M.M. Luo, G. Liu, X.S. Wang, W. Tao, Y.X. Lin, X.Y. Ji, L. Nie, L. Mei, Polydopamine-modified black phosphorous nanocapsule with enhanced stability and photothermal performance for tumor multimodal treatments, Adv. Sci. 5 (10) (2018), 1800510, https://doi.org/10.1002/advs.201800510.

[49] J.D. Shao, H.H. Xie, H. Huang, Z.B. Li, Z.B. Sun, Y.H. Xu, Q.L. Xiao, X.F. Yu, Y.T. Zhao, H. Zhang, H.Y. Wang, P.K. Chu, Biodegradable black phosphorus-based nanospheres for in vivo photothermal cancer therapy, Nat. Commun. 7 (2016), 12967, https://doi.org/10.1038/ncomms12967.

[50] G.B. Qu, W. Liu, Y.T. Zhao, J. Gao, T. Xia, J.B. Shi, L.G. Hu, W.H. Zhou, J.J. Gao, H.Y. Wang, Q. Luo, Q.F. Zhou, S.J. Liu, X.F. Yu, G.B. Jiang, Improved biocompatibility of black phosphorus nanosheets by chemical modification, Angew. Chem., Int. Ed. 56 (46) (2017) 14488–14493, https://doi.org/10.1002/anie.201706228.

[51] W.S. Chen, J. Ouyang, H. Liu, M. Chen, K. Zeng, J.P. Sheng, Z.J. Liu, Y.J. Han, L.Q. Wang, J. Li, L. Deng, Y.N. Liu, S.J. Guo, Black phosphorus nanosheet-based drug delivery system for synergistic photodynamic/photothermal/chemotherapy of cancer, Adv. Mater. 29 (5) (2017), 1603864, https://doi.org/10.1002/adma.201603864.

[52] T. Liu, C. Wang, X. Gu, H. Gong, L. Cheng, X. Shi, L. Feng, B. Sun, Z. Liu, Drug delivery with PEGylated MoS$_2$ nano-sheets for combined photothermal and chemotherapy of cancer, Adv. Mater. 26 (21) (2014) 3433–3440.

[53] C. Zhao, J. Lin, Y. Cai, Y. Zhong, Y. Li, B. Zhou, Evaluation of stability and antitumor activity of two-dimensional black phosphorus modified with positively charged protein, Nanotechnology 34 (33) (2023), 335701, https://doi.org/10.1088/1361-6528/acd647.

[54] Y. Liang, X. Zhou, Q. Xie, H. Sun, K. Huang, H. Chen, W. Wang, B. Zhou, X. Wei, D. Zeng, H. Lin, CD146 interaction with integrin β1 activates LATS1-YAP signaling and induces radiation-resistance in breast cancer cells, Cancer Lett. 546 (2022), 215856, https://doi.org/10.1016/j.canlet.2022.215856.

[55] J. Fang, H. Nakamura, H. Maeda, The EPR effect: unique features of tumor blood vessels for drug delivery, factors involved, and limitations and augmentation of the effect, Adv. Drug Deliv. Rev. 63 (3) (2011) 136–151, https://doi.org/10.1016/j.addr.2010.04.009.

[56] F. Danhier, To exploit the tumor microenvironment: since the EPR effect fails in the clinic, what is the future of nanomedicine? J. Contr. Release 244 (2016) 108–121, https://doi.org/10.1016/j.jconrel.2016.11.015.

[57] Z. Xie, M. Peng, R. Lu, X. Meng, W. Liang, Z. Li, M. Qiu, B. Zhang, G. Nie, N. Xie, H. Zhang, P.N. Prasad, Black phosphorus-based photothermal therapy with aCD47-mediated immune checkpoint blockade for enhanced cancer immunotherapy, Light, Sci. Appl. 9 (2020) 161, https://doi.org/10.1038/s41377-020-00388-3.

[58] K. Richter, M. Haslbeck, J. Buchner, The heat shock response: life on the verge of death, Mol. Cell 40 (2) (2010) 253–266, https://doi.org/10.1016/j.molcel.2010.10.006.

[59] S.A. Hurvitz, R. Hegg, W.P. Chung, S.A. Im, W. Jacot, V. Ganju, J.W.Y. Chiu, B. Xu, E. Hamilton, S. Madhusudan, H. Iwata, S. Altintas, J.W. Henning, G. Curigliano, J.M. Perez-Garcia, S.B. Kim, V. Petry, C.S. Huang, W. Li, J.S. Frenel, S. Antolin, W. Yeo, G. Bianchini, S. Loi, J. Tsurutani, A. Egorov, Y. Liu, J. Cathcart, S. Ashfaque, J. Cortes, Trastuzumab deruxtecan versus trastuzumab emtansine in patients with HER2-positive metastatic breast cancer: updated results from DESTINY-Breast03, a randomised, open-label, phase 3 trial, Lancet 401 (10371) (2023) 105–117, https://doi.org/10.1016/S0140-6736(22)02420-5.